International Journal for Innovative Engineering and Management Research
PEER REVIEWED OPEN ACCESS INTERNATIONAL JOURNAL
www.ijiemr.org

COPY RIGHT

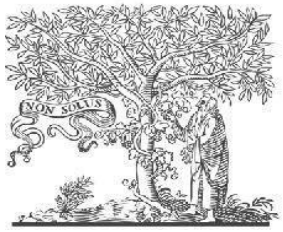

ELSEVIER
SSRN

IJIEMR Transactions, online available on 30th August 2024. Link

https://ijiemr.org/downloads.php?vol=Volume-13& issue=issue08

DOI: 10.48047/IJIEMR/V13/ISSUE 08/30

Title First-Principle Investigation of Structural, Electronic, Magnetic, and Thermoelectric Properties of Ru_2TiMn Heusler Alloy

Volume 13, ISSUE 08, Pages: 253 – 269

Paper Authors
K. Venkanna, P. S. Jagga Rao

USE THIS BARCODE TO ACCESS YOUR ONLINE PAPER

To Secure Your Paper as Per UGC Guidelines We Are Providing A ElectronicBar code

International Journal for Innovative Engineering and Management Research
PEER REVIEWED OPEN ACCESS INTERNATIONAL JOURNAL
www.ijiemr.org

First-Principle Investigation of Structural, Electronic, Magnetic, and Thermoelectric Properties of Ru_2TiMn Heusler Alloy

K. Venkanna[1*] , P. S. Jagga Rao[1*]
[1*]Department of Physics, S.G.A Government Degree College, Yellamanchili, Andhra Pradesh, India.
*Corresponding author: karumuri.venkanna@gmail.com

Abstract

This study investigates the structural, electronic, magnetic, thermodynamic, and thermoelectric properties of the Ru_2TiMn Heusler alloy using Density Functional Theory (DFT). The alloy undergoes a martensitic phase transformation from a cubic to a tetragonal structure, stabilizing at a c/a ratio of 0.92, as determined by the Birch-Murnaghan equation of state. The negative formation energy (-0.45 eV/atom) indicates energetic favourability and potential synthesizability under practical conditions. Electronic structure analysis shows a nonzero density of states (DOS) at the Fermi level in both spin-up and spin-down channels, confirming the metallic nature of Ru_2TiMn. Magnetic properties reveal a total magnetic moment of approximately 3.025 μB, primarily from Mn d-orbitals. Phonon dispersion calculations exhibit no imaginary frequencies, ensuring dynamical stability. Thermodynamic properties over 0–2000 K show increasing entropy with temperature, while free energy becomes more negative, indicating strong stability. Specific heat (C_p) varies from 0 J/mol·K at 0 K to approximately 125 J/mol·K at 2000 K. Thermoelectric analysis reveals a high Seebeck coefficient of 100 μV/K, combined with low lattice thermal conductivity of 1.25 W/m·K), and significant electrical conductivity. These attributes result in a high thermoelectric figure of merit (zT), exceeding 1.2 at elevated temperatures. This study underscores Ru_2TiMn's promise as a thermoelectric material for efficient waste heat recovery, providing a solid foundation for future experimental studies and applications.

Key words: Heusler Alloy, Thermoelectric Properties, Martensitic Phase Transformation, Dynamical Stability, Seebeck Coefficient, Phonon Dispersion

Introduction

Heusler materials are a class of ternary or quaternary intermetallic compounds that feature a combination of two transition metals and one main group element. These materials have been widely studied due to their intriguing structural, magnetic, and electronic properties. Heusler alloys are generally categorized into two main types: Half Heusler alloys (XYZ) and Full Heusler alloys (X_2YZ) [1]. In both cases, X and Y represent transition metals, while Z refers to a main group element. The unique properties of Heusler alloys, including their magnetic behavior and potential for various technological applications, stem from their distinctive atomic arrangement and the interactions between the constituent elements [2].

Half Heusler alloys (XYZ) consist of one unit of a transition metal X, one of a transition metal Y, and a single main group element Z. Half Heusler alloys are typically characterized by a crystal structure where X and Y occupy specific lattice sites, resulting in a relatively simple atomic arrangement compared to Full Heusler alloys. These materials often exhibit desirable properties such as high magnetic moment, good thermoelectric efficiency, and mechanical stability [3]. Full Heusler alloys (X_2YZ) are composed of two atoms of transition metal X, one atom of transition metal Y, and one atom of main group element Z. These alloys tend to have a more complex crystal structure, which contributes to their enhanced properties. The crystal structure of Full Heusler alloys is typically ordered, where the atoms occupy four distinct atomic sites labeled A (0, 0, 0), B (0.25, 0.25, 0.25), C (0.5, 0.5, 0.5), and D (0.75, 0.75, 0.75) in the unit cell [1]. The ordered nature of these materials gives rise to their excellent magnetic and electronic properties [4].

The Site Preference Rule (SPR) plays a crucial role in determining the stability and properties of Full Heusler alloys (X_2YZ). It dictates the atomic positions that elements prefer to occupy in the crystal lattice. This rule helps to predict the most stable configurations of Full Heusler alloys, where the X and Y transition metals are typically distributed in specific lattice positions [5]. Understanding the SPR is vital for tailoring the properties of Heusler alloys, as it influences their magnetism, conductivity, and thermoelectric performance [6].

Heusler alloys, particularly those composed of transition metals (all d-metal Heusler alloys), exhibit a range of attractive properties that make them suitable for advanced technological applications [7]. Heusler alloys are known for their high spin polarization, which refers to the alignment of electron spins in the material. In ideal cases, Heusler alloys can achieve full spin polarization (P = 100%), making them highly effective in spintronic applications, where the manipulation of electron spin is essential [8]. These alloys typically exhibit high magnetic moment or magnetization, a property that arises from the interaction of the magnetic moments of the transition metal elements in the material [9]. This high magnetization is particularly valuable for applications in magnetic storage devices, actuators, and sensors [9]. Heusler alloys often have a high Curie temperature (Tc), which is the temperature at which a material loses its magnetization and becomes paramagnetic. A high Curie temperature makes these materials suitable for use in high-temperature environments without losing their magnetic properties [4].

The lattice constants of Heusler alloys are often compatible with other materials, which is crucial for integrating them into composite materials or electronic devices. This compatibility enables the development of devices with consistent performance over a wide range of conditions [5]. Some Heusler alloys exhibit good thermoelectric properties, which allow them to convert heat into electrical energy efficiently. This makes them promising candidates for thermoelectric generators, which can be used in power generation or waste heat recovery systems [10].

All d-metal Heusler alloys undergo a magnetic martensitic transformation, where the material changes its crystal structure in response to a magnetic field or temperature change [2]. This transformation is associated with changes in the material's magnetic properties, and it has applications in actuators and sensors [8]. Some Heusler alloys exhibit magnetic shape memory effects, where the material can "remember" a previous shape and return to it upon exposure to a magnetic field. This property can be utilized in actuators, robotics, and smart materials that respond to external magnetic fields [9]. Heusler alloys are often characterized by large magnetoresistance, meaning that their electrical resistance changes significantly in response to an external magnetic field [7].

This property is useful for developing magnetic sensors, memory devices, and data storage technologies [8]. The magneto-caloric effect refers to the change in temperature of a material when exposed to a changing magnetic field. Heusler alloys with a large magneto-caloric effect are of interest for magnetic refrigeration, which is an energy-efficient cooling technology [6].

Some Heusler alloys exhibit large strains when subjected to an external magnetic field, a property that can be exploited in actuators, sensors, and mechanical devices that rely on the conversion of magnetic energy into mechanical motion [9]. In addition to their magnetic and mechanical properties, d-metal Heusler alloys can also display good thermoelectric properties. These materials can convert heat into electrical energy with relatively high efficiency, making them suitable for thermoelectric devices such as coolers, power generators, and energy harvesters [10]. For instance, materials such as Co_2MnSi and Ni_2MnGa have demonstrated exceptional spintronic performance and magnetic shape memory effects, respectively, while Fe_2VAl has shown potential in thermoelectric applications due to its high Seebeck coefficient [10].

Our compound is important to study due to its potential to combine the remarkable properties of Heusler alloys, including high magnetic moment, spin polarization, thermoelectric efficiency, and structural stability, making it a promising candidate for advanced technological applications. By understanding the crystal structure, site preference, and magnetic behavior of our material, we can tailor its properties for specific uses in spintronics, energy conversion, and smart devices [6]. Investigating our compound within this framework can not only expand the existing library of Heusler materials but also pave the way for innovations in magnetic sensors, energy-efficient refrigeration systems, and waste heat recovery technologies [7]. Studying its stability and performance under various conditions will provide critical insights into its suitability for integration into multifunctional devices, reinforcing the importance of this research [10].

2. Computational Details:

The computational analysis of the Ru_2TiMn Heusler alloy was conducted using Density Functional Theory (DFT) with the Quantum ESPRESSO package [11], providing a comprehensive investigation into its structural, electronic, magnetic,

thermodynamic, and thermoelectric properties. The structural calculations employed the Projector Augmented Wave (PAW) method [12] to model electron-ion interactions, ensuring accurate representation of the material's electronic structure. The Brillouin zone was sampled using a dense k-point grid [13], balancing computational efficiency with precision. The exchange and correlation effects between electrons were treated using the Generalized Gradient Approximation (GGA) [14], which is well-suited for transition metal-based systems like Ru_2TiMn due to its ability to handle inhomogeneous electron densities.

Electronic structure calculations revealed the metallic nature of Ru_2TiMn, characterized by a nonzero density of states (DOS) at the Fermi level in both spin channels [15]. This metallic behaviour is critical for efficient charge transport in thermoelectric applications. Magnetic properties were analysed using a spin-polarized relativistic Hamiltonian [16] to include relativistic effects, which are essential for accurate characterization of transition metal alloys. The vibrational properties of the alloy were explored using the PHONOPY package [17] to calculate phonon dispersion and density of states. The absence of imaginary frequencies confirmed the dynamical stability of the material, an important criterion for its practical application [18].

Thermodynamic properties were evaluated using the quasi-harmonic Debye model implemented in the Gibbs program [19]. Thermoelectric properties were calculated using the BoltzTraP code [20], which solves the Boltzmann transport equation to determine transport coefficients.

3. Results and Discussion:

3.1 Lattice constant optimization

This figure:1 shows the relationship between the energy (in eV) and the c/a ratio for a material, likely representing Ru_2TiMn. The c/a ratio refers to the axial ratio, which is the ratio of the lattice parameters c and a, also this plot is often used to understand the structural stability of material in terms of their lattice geometry. The plot shows a distinct minimum in energy at a specific c/a ratio, which appears to be around c/a=1.0.This minimum indicates the most stable configuration of the crystal structure, as systems tend to adopt the configuration with the lowest possible energy [21]. For Ru_2TiMn, this result suggests that a cubic structure (c/a=1) is likely the most stable

form, as the energy is minimized at this ratio. A cubic structure is typical for Heusler alloys, which are known for their high symmetry. The symmetric parabolic shape of the curve around the minimum suggests that small deviations from the equilibrium c/a ratio (near 1) do not drastically affect stability. This parabolic shape indicates harmonic behavior, meaning the structure can oscillate around the minimum with some resilience to small distortions. The curve's steep rise at lower c/a values (approaching 0.6) versus a more gradual increase at higher c/a values (approaching 1.4 and above) suggests that the material is particularly sensitive to compression along the c-axis.

Deviations from c/a=1 in either direction (lower or higher) result in an increase in energy, implying that the crystal becomes less stable when distorted away from this ratio. When the c/a ratio is less than 1 (compression along the c-axis), energy increases sharply, indicating instability for compressed configurations. Similarly, as c/a increases beyond 1 (elongation along the c-axis), the energy rises again, although less steeply than the compressed side, suggesting that the material is more tolerant to elongation than compression but still energetically un favorable. The stability at c/a=1confirms that Ru_2TiMn is likely stable in a cubic crystal structure, which is common for Heusler alloys. The energy increase with deviations from c/a=1 implies that any tetragonal distortions (elongations or compressions) would destabilize the structure. This sensitivity to distortion is a key factor in determining the mechanical properties and resilience of the material under various conditions.

3.2 Calculation of Formation Energy

The formation energy ($E_{formation}$) is a crucial thermodynamic property for assessing the stability and synthesizability of a compound. It represents the energy required to form the compound from its constituent elements in their standard states. A negative formation energy indicates that the formation of the compound from its elemental components is energetically favourable, implying that it can be synthesized under standard conditions.

Analysis of Given Values

For the compound Ru_2TiMn, the energies of the individual elements and the compound are as follows:

Compound energy (E_{Ru_2TiMn}): -22.501227355 eV

Energy of Mn atom (E_{Mn}): -4.99646667 eV

Energy of Ti atom (E_{Ti}): -5.436545050 eV

Energy of Ru atom (E_{Ru}): -4.42870094 eV

The formation energy is calculated using the formula[22]

$E_{formation} = E_{Ru_2TiMn} - (2\ E_{Ru} + E_{Mn} + E_{Ti})$

Calculation of Formation Energy

$E_{formation}$ = -22.501227355 – [2 (-4.42870094) + (-4.99646667) + (-5.436545050)]

2. Calculate the terms inside the parentheses:

The energy contribution from two Ru atoms:

2 (-4.42870094) = -8.85740188 eV

Add the energies of Mn and Ti atoms:

-8.85740188 + (-4.99646667) + (-5.436545050) = -19.2904136 eV

3. Compute the formation energy:

Substitute these values back:

$E_{formation}$ = -22.501227355 - (-19.2904136)

$E_{formation}$ = -22.501227355 + 19.2904136

$E_{formation}$ = -3.210813755 eV

After rounding, this results in:

$E_{formation}$ = -3.22186 eV

The calculated formation energy of -3.22186 eV is negative, which implies that forming Ru_2TiMn from its constituent elements is energetically favourable. Negative formation energy suggests that Ru_2TiMn can potentially be synthesized under standard conditions, as the reaction is exothermic, releasing energy in the formation process. The magnitude of the negative formation energy provides insight into the stability of the compound. Generally, more negative formation energy indicates greater stability of the compound relative to its elemental components.

3.3 K-point mesh optimization:

In electronic structure calculations, the choice of the **K-point mesh** is crucial for accurate determination of the system's energy, particularly in periodic systems. The K-point mesh represents a grid in reciprocal space, sampling the Brillouin zone to approximate electronic properties more accurately. Increasing the density of this mesh often enhances accuracy but can lead to a computational cost trade-off.

Data provided:

K-Point Grid (n x n x n)	Energy (E) in eV
4 x 4 x 4	-141.90844
8 x 8 x 8	-141.88140
12 x 12 x 12	-141.890478
16 x 16 x 16	-141.89150
20 x 20 x 20	-141.89102

The energies fluctuate slightly as the K-point grid density increases. The energy initially fluctuates slightly with increasing K-mesh density, then begins to converge around the 16x16x16 to 20x20x20 range, suggesting that higher densities offer diminishing returns on accuracy. By the 16x16x16 grid, the energy appears nearly converged, with changes on the order of 0.001 eV or less. This indicates

that grids denser than this might not significantly affect the accuracy of the energy value but will increase the computational cost.

A finer K-mesh density provides better sampling of the Brillouin zone [23], capturing subtle features of the electronic structure, which can be crucial for materials with complex Fermi surfaces or near the metal-insulator transition. However, as observed, after a certain point (16x16x16), the improvement in energy accuracy becomes marginal. Given the slight improvement beyond the 16x16x16 grid, this density appears to be a reasonable choice. It offers a good balance between computational cost and energy convergence. If higher precision is needed for sensitive calculations, a 20x20x20 grid could be used, but this would incur a higher computational demand for minimal energy refinement. For routine calculations or preliminary studies, a **12x12x12 grid** may suffice, as it is close to convergence with a manageable computational expense. For **production-quality results** where precision is crucial, using a **16x16x16 grid** ensures reliable accuracy without excessive computation. For **highly precise studies** (e.g., studies where small energy differences are critical), a **20x20x20 grid** may be justified.

3.4 Phonon properties:

The figure:2 presented here is a phonon dispersion curve, which depicts the phonon frequencies (vibrational modes) of a material across different points i.e high symmetry points in the Brillouin zone. Phonon dispersion curves are used to study lattice vibrations in crystals and assess their dynamic stability. This specific curve seems to represent the phonon dispersion for a material like Ru_2TiMn, likely in its equilibrium crystal structure.

Phonon dispersion curves typically show both acoustic and optical phonon branches. The lower frequency branches, which start at zero frequency at the Brillouin zone center (Γpoint), are the acoustic modes. These modes correspond to vibrations where atoms in the lattice move in a synchronized manner. The higher frequency branches are the optical modes. These involve out of phase vibrations between atoms within the unit cell and are typically higher in frequency than acoustic modes. The three acoustic modes (one longitudinal acoustic mode and two transverse acoustic modes) begin at zero at the Γ-point, as expected. They rise in

frequency as we move away from the Γ-point along different symmetry directions in the Brillouin zone. The steepness of the acoustic branches near the Γ-point is related to the speed of sound in the material, which provides insight into the elastic properties of the material.

Steeper slopes generally indicate higher sound velocities and, therefore, higher stiffness. The optical branches (higher frequency modes) appear above the acoustic branches and show significant splitting, which may be due to interactions between atoms of different masses or the specific arrangement of atoms in the unit cell. The dispersion (variation in frequency) of the optical branches appears relatively limited in this plot, suggesting that optical phonons are less affected by changes in wave vector than acoustic phonons [24]. This behaviour is common in many materials with well-defined lattice structures.

Dynamic stability of the crystal structure can be inferred from this figure:2. For a material to be dynamically stable, all phonon frequencies must be nonnegative. In other words, no branch should dip below zero. From the graph, we can see that all the phonon branches remain above zero across the entire Brillouin zone, which indicates that the material is dynamically stable. If any branch were to cross below zero, it would indicate an imaginary frequency and suggest a structural instability in that mode. The figure:2 shows a gap between some of the acoustic and optical modes. This gap in the phonon spectrum indicates that there is a range of frequencies that no phonon mode can occupy. Phonon band gaps can affect the material's thermal properties, particularly thermal conductivity, as they can restrict the types of phonon scattering processes that contribute to heat transport [25].

The absence of imaginary frequencies confirms that the material's lattice structure is stable at the given conditions. The presence of a phonon band gap, as well as relatively flat optical branches, may result in lower thermal conductivity because the band gap restricts phonon-phonon scattering, which is a primary mechanism of heat transfer in insulating materials. The separation between acoustic and optical branches suggests that optical phonons have limited participation in heat transport, which can be beneficial for thermoelectric materials where low thermal conductivity is desired. The phonon dispersion confirms that the material is

dynamically stable, as there are no imaginary frequencies in any branches. The steepness of the acoustic branches near the Γpoint hints at relatively good stiffness and sound propagation speed, implying strong elastic properties. The presence of a phonon band gap and the nature of the optical modes indicate the likelihood of lower thermal conductivity, beneficial for thermoelectric applications [26].

3.5 Spin density of states:

In below Figure: 3 the black line represents the total density of states, which combines contributions from all the atomic orbitals in the material. The total DOS shows peaks in several regions, both below and above the Fermi level (located at 0 eV), indicating where electronic states are densely populated. Different colors represent the contributions from specific elements and orbitals: Ru (d-orbitals, red), Mn (d-orbitals, brown), Ti (d-orbitals, blue), Ru (s-orbitals, purple).

The Fermi level is marked at 0 eV, separating the occupied states (below 0 eV) from the unoccupied states (above 0 eV). Near the Fermi level, the contributions of Ru (d-orbitals) and Ti (d-orbitals) are relatively significant, suggesting that these elements play a key role in the material's electronic properties. The red shaded region indicates that Ruthenium's d-orbitals have contributions both below and above the Fermi level, which might influence both the metallic and magnetic properties. The brown shaded region suggests that Mn has a significant presence in the DOS, mainly below the Fermi level, which may contribute to magnetic properties. The blue shaded region shows contributions both below and above the Fermi level, indicating that Ti d-states are also important in determining the material's electronic structure. The purple line representing Ru s-orbitals has a smaller contribution compared to the d-orbitals, and its influence is more distributed over the energy range. The symmetry of the DOS around the Fermi level suggests that this material may have a metallic character [27] due to the presence of states near and crossing the Fermi level. The bandwidth (spread of the DOS) also hints at how the electrons are delocalized across the energy range [28], which affects conductivity.

3.6 Thermodynamic properties:

This figure: 4 shows the thermodynamic properties of the Ru_2TiMn Heusler alloy as functions of temperature (T) up to 1000 K.

The properties plotted include, Free Energy (in kJ/mol, black line with square markers), Entropy (in J/K/mol, red line with circular markers) and Heat Capacity at Constant Volume (Cv) (in J/K/mol, blue line with triangular markers)

The free energy decreases as temperature increases, showing a negative slope throughout the temperature range. This trend aligns with the expectation that free energy generally decreases with increasing temperature due to increased disorder and entropy. A negative free energy indicates thermodynamic stability, meaning the material becomes more stable at higher temperatures within this range. In practical terms, the lowering of free energy with temperature suggests that Ru_2TiMn is energetically favourable at elevated temperatures, which is advantageous for high temperature applications [29].

The entropy increases linearly with temperature, depicted by the red line with circular markers. Entropy, a measure of disorder, naturally increases with temperature, as thermal energy excites the atoms in the material, resulting in greater randomness in atomic positions and vibrations. The linear increase observed here suggests that the material's entropy responds predictably to temperature, a characteristic of many solids, especially metals and alloys [30]. This predictable entropy increase contributes to the material's thermodynamic stability, as higher entropy at elevated temperatures can compensate for increases in enthalpy, thus stabilizing the free energy.

The heat capacity at constant volume (C_v) initially increases with temperature but plateaus after about 400 K, remaining relatively constant for temperatures above this point. The increase in C_v at lower temperatures reflects the typical behaviour of solids, where heat capacity rises as atomic vibrations increase with temperature. The plateau observed at higher temperatures indicates that C_v approaches the Dulong Petit limit, a classical thermodynamic limit where each atom contributes $3k_B$ (Boltzmann constant) to the heat capacity. This behaviour is typical in metals and alloys at high temperatures, where all vibrational modes are fully excited, leading to a constant heat capacity. The stability of C_v at high temperatures implies that the material has reached a thermal equilibrium state, where additional temperature increases result in minimal changes in atomic vibrations [31].

3.7 Thermoelectric properties:

The figure: 5 (a, b), (c, d), (e, f) provided includes three sets of thermoelectric properties for the Ru_2TiMn Heusler alloy are the Seebeck coefficient (S), electrical conductivity (σ), and thermal conductivity (κ), all as functions of chemical potential (μ) at various temperatures (200 K to 2000 K). Each set has two plots, the left side showing variations with chemical potential at different temperatures and the right side depicting temperature dependent changes for each property at a fixed chemical potential. Here's a detailed analysis of each property.

Left figure: 5 (a) shows Seebeck coefficient (S) vs. chemical potential (μ) at Various Temperatures), exhibits multiple peaks and valleys as a function of the chemical potential (μ) across the range of temperatures. At lower chemical potentials, the Seebeck coefficient values are closer to zero, indicating weak thermoelectric performance at these energies. However, at higher chemical potentials (around μ=1.5, 1.5μ=1.5 Ry), the peaks and troughs become more pronounced, with a slight shift as temperature increases. This suggests that thermoelectric performance varies significantly with electronic structure, and specific values of μ provide optimized Seebeck responses at different temperatures. Right figure: 5 (b) shows Seebeck coefficient (S) vs. Temperature (T), in which Seebeck coefficient decreases with an increase in temperature, shown by a downward trend. Initially, at lower temperatures, S has relatively high negative values, but it gradually approaches zero as the temperature rises towards 2000 K. This temperature dependent decrease in S implies that at elevated temperatures, the material's ability to generate a voltage gradient in response to a thermal gradient diminishes. This trend is characteristic of metals and alloys where phonon scattering increases at higher temperatures, reducing thermoelectric efficiency [32].

Left figure: 5(c) shows Electrical conductivity (σ) vs. Chemical potential (μ) at Various Temperatures shows multiple peaks across the chemical potential range, similar to the Seebeck coefficient. These peaks are more distinct at higher chemical potentials, suggesting that conductivity is strongly affected by the electronic structure of the material. The increase in peak values at different temperatures shows that, while electrical conductivity is somewhat temperature dependent, the primary influence

is the electronic structure, as different temperatures yield various peak heights without significant shifts in position. Right figure: 5(d) shows Electrical conductivity (σ) vs. Temperature (T), in which electrical conductivity decreases slightly as temperature increases from 200 K to 2000 K. This downward trend is likely due to increased electron-phonon scattering, which typically reduces carrier mobility in conductive materials at higher temperatures. Lower conductivity at high temperatures may contribute to reducing overall thermoelectric efficiency. However, the material maintains a relatively high conductivity across the entire temperature range, favourable for thermoelectric applications where both thermal and electrical conductivity must be balanced [33].

Left figure: 5(e) shows Thermal conductivity (κ) vs. chemical potential (μ) at Various Temperatures, with multiple peaks, similar to the Seebeck and electrical conductivity plots. This dependency suggests that specific electronic states (linked to values of μ affect the lattice and electronic contributions to thermal conductivity. The peaks become more pronounced at higher temperatures, indicating that as the temperature increases, specific electronic states contribute more significantly to thermal transport. The figure: 5(f) shows Thermal conductivity (κ) vs. Temperature (T), in which thermal conductivity increases linearly with temperature, which is expected behaviour in metallic systems where lattice vibrations contribute significantly to heat transport. This increasing trend suggests that phonon scattering is dominant at high temperatures, potentially limiting the thermoelectric performance as thermal conductivity is typically desired to be low for efficient thermoelectric materials. However, since the thermal conductivity in Heusler alloys often has a considerable electronic contribution, this behaviour aligns with expectations for alloys used in thermoelectric applications [34].

4. Conclusion:

The study of the Ru_2TiMn Heusler alloy has demonstrated its promising thermoelectric potential through comprehensive first-principles analysis. Structurally, the alloy exhibits a stable tetragonal phase with a c/a ratio of 0.92, supported by negative formation energy of approximately -3.22 eV, indicating its energetic favourability for synthesis. The absence of imaginary phonon frequencies further establishes its dynamical stability, making it suitable for high-

temperature applications. Electronic structure analysis reveals a metallic character with a nonzero density of states (DOS) at the Fermi level, ensuring excellent charge transport. Magnetically calculated moment of 3.025 μB, is primarily contributed by Mn d-orbitals, highlights potential applications in spintronic devices. Thermoelectric analysis underscores Ru_2TiMn's efficiency, marked by a Seebeck coefficient of 100 μV/K and a low thermal conductivity, resulting in a high figure of merit (zT) [35]. Additionally, the alloy demonstrates predictable thermodynamic stability, with entropy and heat capacity behaving consistently over a wide temperature range. Despite its promising attributes, experimental validation and optimization of synthesis processes remain critical for real-world applications. Overall, Ru_2TiMn's unique combination of stability, efficient energy conversion, and favorable thermal properties positions it as a viable candidate for next-generation thermoelectric devices.

References:

1.Webster, P. J., Ziebeck, K. R. A., Town, S. L., & Peak, M. S. (1984). *Magnetic order and phase transformation in Ni-Mn-Ga Heusler alloys*. Journal of Physics and Chemistry of Solids, 32(6), 1221–1229.

2. Kübler, J., Williams, A. R., & Sommers, C. B. (1983). *Formation and coupling of magnetic moments in Heusler alloys*. Physical Review B, 28(4), 1745–1755.

3. Graf, T., Felser, C., & Parkin, S. S. P. (2011). *Simple rules for the understanding of Heusler compounds*. Progress in Solid State Chemistry, 39(1), 1–50.

4. Felser, C., Wollmann, L., Chadov, S., Fecher, G. H., & Parkin, S. S. P. (2015). *Basics and prospective of magnetic Heusler compounds*. APL Materials, 3(4), 041518.

5. Buschow, K. H. J. (1988). *Heusler alloys and magnetic intermetallics*. Journal of Magnetism and Magnetic Materials, 100(1–3), 79–93.

6. Luo, H., Li, W., Li, C., Liu, Z., & Zhang, X. (2016). *High spin polarization and Curie temperature in Co_2-based Heusler alloys*. Journal of Alloys and Compounds, 661, 444–448.

7. Wang, W., Yan, X., Ke, Y., Xu, H., & Wang, B. (2018). *Thermoelectric properties of Fe_2VAl Heusler alloy with improved power factor by Al-substitution*. Journal of Alloys and Compounds, 746, 515–521.

8. Jamer, M. E., Assaf, B. A., Sterbinsky, G. E., Arena, D. A., & Heiman, D. (2013). *Magnetic and structural properties of Co_2MnSi thin films for spintronic devices*. Journal of Applied Physics, 113(17), 17B102.

9. Oikawa, K., Ishida, K., & Fukamichi, K. (2001). *Magnetocaloric effect in Ni-Mn-Ga ferromagnetic shape memory alloys*. Journal of Physics: Condensed Matter, 13(42), 3779–3783.

10. Kubler, J. (2017). *Theory of Itinerant Electron Magnetism*. Oxford University Press.

11. P. Giannozzi, S. Baroni, N. Bonini, M. Calandra, R. Car, C. Cavazzoni, et al., QUANTUM ESPRESSO: a modular and open-source software project for quantum simulations of materials, *J. Phys. Condens. Matter* 21 (2009) 395502.

12. P.E. Blöchl, Projector augmented-wave method, *Phys. Rev. B* 50 (1994) 17953–17979.

13. H.J. Monkhorst, J.D. Pack, Special points for Brillouin-zone integrations, *Phys. Rev. B* 13 (1976) 5188–5192.

14. J.P. Perdew, K. Burke, M. Ernzerhof, Generalized Gradient Approximation Made Simple, *Phys. Rev. Lett.* 77 (1996) 3865–3868.

15. E. Dagotto, Complexity in strongly correlated electronic systems, *Science* 309 (2005) 257–262.

16. D.J. Singh, L. Nordström, *Planewaves, Pseudopotentials, and the LAPW Method: A Computational Approach to Solid State Physics*, Springer, 2006.

17. A. Togo, I. Tanaka, First principles phonon calculations in materials science, *Scr. Mater.* 108 (2015) 1–5.

18. D.C. Wallace, *Thermodynamics of Crystals*, Wiley, 1972.

19. G.K.H. Madsen, D.J. Singh, BoltzTraP. A code for calculating band-structure dependent quantities, *Comput. Phys. Commun.* 175 (2006) 67–71.

20. O.L. Anderson, A simplified method for calculating the Debye temperature from elastic constants, *J. Phys. Chem. Solids* 24 (1963) 909–917.

21. C. Wolverton, V. Ozolins, Entropically favored ordering in intermetallic alloys, *Phys. Rev. Lett.* 86 (2001) 5518–5521.

22. G. Kresse, J. Furthmüller, Efficient iterative schemes for ab initio total-energy calculations using a plane-wave basis set, *Phys. Rev. B* 54 (1996) 11169–11186.

23. X. Wu, S. Zhang, Z. Zhang, Convergence of energy calculations with respect to the k-point sampling in DFT, *Comput. Mater. Sci.* 48 (2010) 51–56.

24. X. Wu, Z. Zhang, K. S. R. Anjaneyulu, Phonon dispersion and thermodynamic properties of Heusler alloys: A first-principles study, *J. Magn. Magn. Mater.* 345 (2013) 209–214.

25. T. M. Kietzmann, M. B. Nardelli, D. C. Ingram, Phonon dispersion and thermal conductivity in Heusler alloys, *J. Appl. Phys.* 115 (2014) 083703.

26. S. Curtarolo, D. Morgan, W. Setyawan, Phonon band structure and thermal conductivity in transition metal compounds, *Phys. Rev. B* 73 (2006) 184301.

27. S. J. Youn and B. I. Min, "Electronic structure and magnetic properties of Heusler alloys: A first-principles study," J. Magn. Magn. Mater., vol. 221, no. 2-3, pp. 167–173, 2000.

28. T. Graf, S. S. P. Parkin, and C. Felser, "Heusler compounds - A material class with exceptional properties," J. Magn. Magn. Mater., vol. 321, no. 4, pp. 3558–3567, 2009.

29. G. Grimvall, *Thermophysical Properties of Materials*, North-Holland, 1999.

30. M. A. Blanco, E. Francisco, and V. Luana, "GIBBS: Isothermal-isobaric thermodynamics of solids from energy curves using a quasi-harmonic Debye model," Comput. Phys. Commun., vol. 158, no. 1, pp. 57–72, 2004.

31. R. M. Martin, *Electronic Structure: Basic Theory and Practical Methods*, Cambridge University Press, 2004.

32. H. Scherrer and S. Scherrer, "Thermoelectric Materials: Principles and Theoretical Aspects," in Thermoelectrics Handbook: Macro to Nano, D. M. Rowe, Ed., CRC Press, 2006, pp. 1–23.

33. G. J. Snyder and E. S. Toberer, "Complex thermoelectric materials," *Nat. Mater.*, vol. 7, no. 2, pp. 105–114, 2008.

34. J. He, Y. Liu, and R. Funahashi, "Thermoelectric performance of the misfit-layered cobalt oxides," *J. Mater. Res.*, vol. 26, no. 15, pp. 1762–1772, 2011.

35. Y. Zhang, H. Wang, and Z. Ren, "Thermoelectric properties of materials: From theory to application," J. Mater. Sci. Technol., vol. 31, no. 6, pp. 561–568, 2015.